Journal of Sound and Vibration (2003) **259**(3), 541–557
doi:10.1006/jsvi.2002.5088, available online at http://www.idealibrary.com on IDEAL®

CHAOTIC AND NON-LINEAR DYNAMIC ANALYSIS OF A TWO-AXIS RATE GYRO WITH FEEDBACK CONTROL MOUNTED ON A SPACE VEHICLE

H.-H. CHEN

Department of Mechanical Engineering, HsiuPing Institute of Technology, No. 11, *Gungye Road, Dali City, Taichung, Taiwan* 412, *Republic of China. E-mail: richard@mail.hit.edu.tw*

(*Received* 27 *September* 2001, *and in final form* 2 *April* 2002)

An analysis is presented in this paper for a two-axis rate gyro subjected to linear feedback control mounted on a space vehicle, which is spinning with uncertain angular velocity $\omega_Z(t)$ about its spin of the gyro. For the autonomous case in which $\omega_Z(t)$ is steady, the stability analysis of the system is studied by Routh–Hurwitz theory. For the non-autonomous case in which $\omega_Z(t)$ is sinusoidal function, this system is a strongly non-linear damped system subjected to parametric excitation. By varying the amplitude of sinusoidal motion, periodic and chaotic responses of this parametrically excited non-linear system are investigated using the numerical simulation. Some observations on symmetry-breaking bifurcations, period-doubling bifurcations, and chaotic behavior of the system are investigated by various numerical techniques such as phase portraits, Poincaré maps, average power spectra, and Lyapunov exponents. In addition, some discussions about chaotic motions of this system can be suppressed and changed into regular motions by a suitable constant motor torque are included.

1. INTRODUCTION

A number of studies over the past few decades have shown that the chaotic phenomena are observed in many physical systems with non-linearity and external excitation [1–3]. The non-linearity of a system, through the various system parameters, exhibits a variety of non-linear behaviors such as jump phenomenon, multiple attractors, subharmonic vibrations, symmetry-breaking bifurcations, period-doubling bifurcations, crisis and chaos [4–7]. In addition, a symmetry-breaking bifurcation occurring before a period-doubling bifurcation, and the appearance of chaos amidst a cascade of period-doubling bifurcations have been observed in driven damped pendulums or Duffing's oscillators by MacDonald [8] and Räty [9]. The bifurcation behaviors mentioned above occur at the boundaries of stability regions. Therefore, an analysis of instability regions in parametric space is a critical problem. In a gyroscopic system, a single-axis rate gyro mounted on a space vehicle free to move in various ways also exhibits complex non-linear and chaotic motions. Its stability was broadly characterized into the stable regions in which the angular velocity of a given vehicle was measured by Singh [10] and Ge *et al.* [11]. The non-linear nature and chaotic motion of a single-axis rate gyro were investigated by Ge and Chen [12, 13] when the vehicle is spinning sinusoidally with respect to the spin axis of the gyro. This system is characterized by parametric excitation and exhibits complex non-linear phenomena in the presence of sinusoidal excitation, including subharmonic vibrations, Hopf bifurcation, symmetry-breaking bifurcations, a series of period-doubling bifurcations, and chaos. In

0022-460X/02/$35.00

practice, chaotic motions are undesirable in many mechanical systems. Ge and Chen [14] used resonant parametric perturbations to change a chaotic motion into a regular one. In this paper, an analysis is presented of a two-axis rate gyro subjected to linear feedback control mounted on a space vehicle that is spinning with an uncertain angular velocity $\omega_Z(t)$ about the spin of the gyro. This is a two-degree-of-freedom system subjected to the complex non-linear terms and parametric excitation. Here, Routh–Hurwitz theory [15] is applied to analyze the stability of the autonomous case in which $\omega_Z(t)$ is steady. For the non-autonomous case in which $\omega_Z(t)$ is sinusoidal function, a number of numerical techniques are used to detect the existence of symmetry-breaking bifurcations, period-doubling bifurcations, and chaos of the parametrically excited non-linear system. The natures of the periodic and chaotic motions are shown in phase plane diagrams, Poincaré maps, and average power spectra. The qualitative bifurcation diagrams, parametric diagrams and quantitative Lyapunov exponents in parametric space are also computed to determine the values of birfurcation points as well as chaos onset. In addition, the chaotic motions of this system can be suppressed and changed into regular motions by a suitable constant motor torque.

2. EQUATIONS OF MOTION

We consider the model of a two-axis rate gyro mounted on a space vehicle as shown in Figure 1. Let X, Y, Z be a set of axes attached to the platform and ξ, η, ζ be gimbal axes. The rotor is mounted in the inner gimbal that can turn about axis X with rotational angle θ. The rotation of the inner gimbal is resisted by the damping torque $d_1\dot{\theta}$ and the control-motor torque T_c. The outer gimbal rotates about axis Y with rotational angle ϕ, and motion about this axis is also resisted by torsional spring and damping torques defined by $k_2\phi$ and $d_2\dot{\phi}$, respectively. Using Lagrange's equation [15], the differential equations of a two-axis gyro with feedback control was derived as follows (see Appendix A(I) for detail):

$$(A + A_1)[\ddot{\theta} - (\omega_X \sin\phi + \omega_Z \cos\phi)\dot{\phi} + (\dot{\omega}_X \cos\phi - \dot{\omega}_Z \sin\phi)] - (A + B_1 - C_1)\omega_\eta\omega_\xi - (-\omega_\eta)H_c + d_1\dot{\theta} = T_c, \tag{1}$$

$$\mathrm{d}/\mathrm{d}t[(A + B_1)\omega_\eta \cos\theta - C_1\omega_\zeta \sin\theta + A_2(\dot{\phi} + \omega_Y) - \sin\theta H_c] + d_2(\dot{\phi} + \omega_Y) + k_2\phi = 0, \tag{2}$$

where $\dot{\theta} = \mathrm{d}\theta/\mathrm{d}t$, $\dot{\phi} = \mathrm{d}\phi/\mathrm{d}t$, $H_c = [C(\omega_\zeta + \dot{\psi})] = const.$, $\omega_\xi = \dot{\theta} + (\omega_X \cos\phi - \omega_Z \sin\phi)$, $\omega_\eta = (\dot{\phi} + \omega_Y)\cos\theta + (\omega_X \sin\phi + \omega_Z \cos\phi)\sin\theta$, $\omega_\zeta = -(\dot{\phi} + \omega_Y)\sin\theta + (\omega_X \sin\phi + \omega_Z \cos\phi)\cos\theta$. ω_X, ω_Y, ω_Z denote the angular velocity components of the platform along output axis X, input axis Y, and normal axis Z respectively. A, $B(=A)$, C and A_1, B_1, C_1 denote the moments of inertia of rotor and inner gimbal about ξ, η, and ζ respectively. A_2 denotes the moment of inertia of the outer gimbal about axis Y. T_c is the control-motor torque along the output axis of the system to balance the corresponding gyroscopic torque. The torque and electric current of control-motor can be modelled by the following relationship:

$$T_c = K_T I, \qquad L\dot{I} + RI = K_a(\theta_d - \theta) - K_0\dot{\theta}, \tag{3, 4}$$

where electromotive force proportional to the difference between the prescribed motion $\theta_d(t)$ and the rotational angle θ, that is $u = K_a(\theta_d - \theta)$, is applied to the control-motor. I, R, L, and K_0 are the current, resistance, inductance, and back-electromotive constant of the

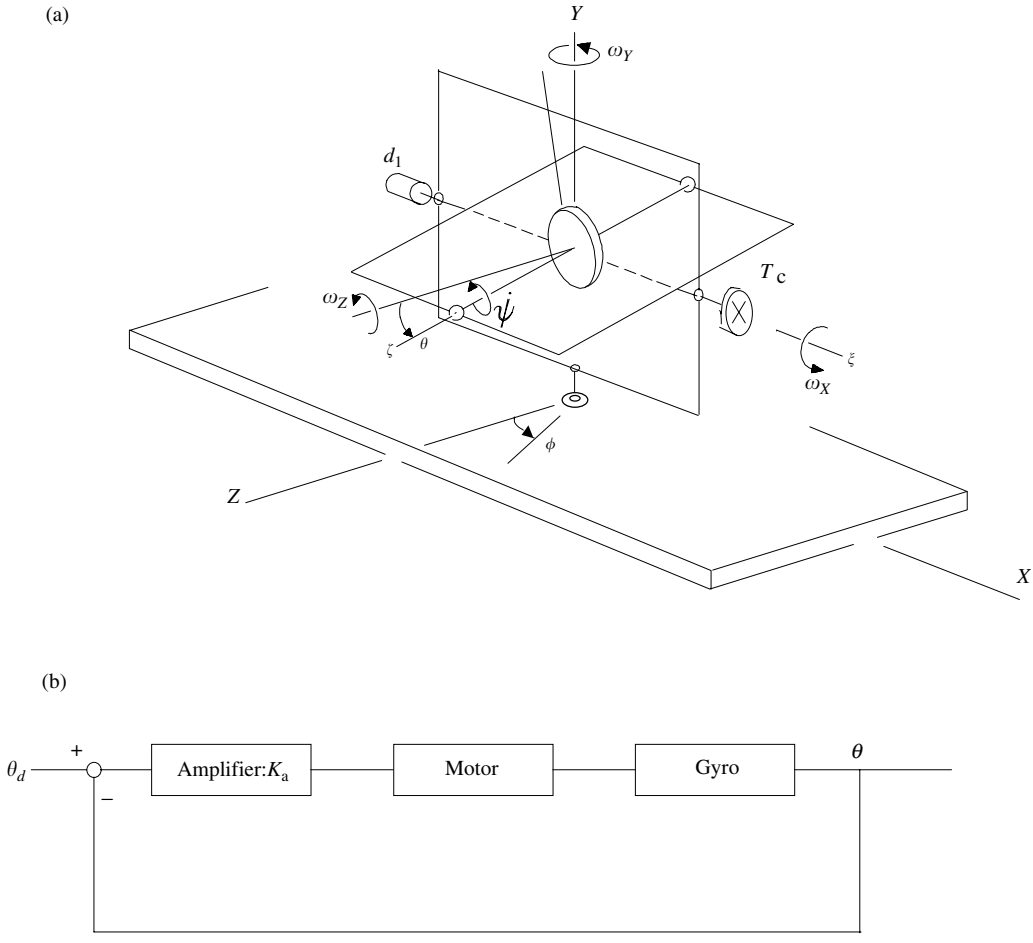

Figure 1. The feedback system (a) the rate gyro; (b) the block diagram.

control-motor; K_T denotes the torque constant of the control-motor. The prescribed motion of the gyro is desired to be fixed at the origin, i.e., $\theta_d = 0$, in which the relationship of the output angle θ proportional to the input angular velocity ω_Y is held.

Considering both the mechanical time constant is much larger than the electrical time constant and the effect of back electromotive force is to be neglected, equations (3) and (4) can be simplified by the following relationship: $T_c = -K_T K_a \theta / R = -k_1 \theta$. Equations (1)–(4) thus represent a feedback control system in which position feedback is applied to the gyro motion.

3. STABILITY ANALYSIS

Firstly, we are interested in the stability of the equilibrium point $(\theta, \dot{\theta}, \phi, \dot{\phi}) = (0, 0, 0, 0)$, which is a measuring datum point of the device, of this gyro when angular velocity along both input and output axes are zero, i.e., $\omega_Y = 0$ and $\omega_X = 0$. For the autonomous system $\omega_Z(t) = \omega_{Z0} = const.$, the stability of the origin of the system is investigated as follows. Let

the disturbed motion of the origin be $\theta = 0 + x_1$, $\dot{\theta} = 0 + x_2$, $\phi = 0 + x_3$, $\dot{\phi} = 0 + x_4$, where x_1, x_2, x_3, x_4 are disturbances, then the differential equations (1)–(4) for disturbances are

$$\dot{x}_1 = x_2, \qquad \dot{x}_2 = F_1(x_1, x_2, x_3, x_4), \qquad \dot{x}_3 = x_4, \qquad \dot{x}_4 = F_2(x_1, x_2, x_3, x_4) \text{ or } \dot{X} = \mathbf{F}, \tag{5}$$

where $\mathbf{X} = [x_1, x_2, x_3, x_4]^{\mathrm{T}}$, $\mathbf{F} = [x_2, F_1, x_4, F_2]^{\mathrm{T}}$, $F_i(x_1, x_2, x_3, x_4)$, $i = 1, 2$, are shown in Appendix B.

The origin $(x_1, x_2, x_3, x_4) = (0, 0, 0, 0)$ is a trivial solution of equation (5). Expanding equation (5) about the origin, we obtain

$$\dot{X} = \mathbf{J}\mathbf{X} + \mathbf{N}_F, \tag{6}$$

where $\mathbf{J} = \partial\mathbf{F}/\partial\mathbf{X}|_{\mathbf{X}=\mathbf{0}}$ is the Jacobian matrix of equation (5) and $\mathbf{N}_F = \mathbf{F} - \mathbf{J}\mathbf{X}$ represents higher order terms in x_i. Assuming that the perturbations are sufficiently small to permit higher order terms in x_i to be ignored, the Routh–Hurwitz criterion [15] is applied to check the stability of the system.

The Jacobian matrix form $\mathbf{J}$ is

$$\mathrm{J} = \begin{bmatrix} 0 & 1 & 0 & 0 \\ a_{21} & a_{22} & 0 & a_{24} \\ 0 & 0 & 0 & 1 \\ 0 & a_{42} & a_{43} & a_{44} \end{bmatrix}, \tag{7}$$

where

$$a_{21} = [(A + B_1 - C_1)\omega_{Z0}^2 - H_c\omega_{Z0} - k_1]/(A + A_1), \qquad a_{22} = -d_1/(A + A_1),$$

$$a_{24} = [(2A + A_1 + B_1 - C_1)\omega_{Z0} - H_c]/(A + A_1),$$

$$a_{42} = -[(2A + A_1 + B_1 - C_1)\omega_{Z0} - H_c]/(A + B_1 + A_2),$$

$$a_{43} = [(A + B_1 - C_1)\omega_{Z0}^2 - H_c\omega_{Z0} - k_2]/(A + B_1 + A_2), \qquad a_{44} = -d_2/(A + B_1 + A_2)$$

and the characteristic equation of $\mathbf{J}$ is

$$\lambda^4 + (-a_{22} - a_{44})\lambda^3 + (-a_{43} - a_{21} + a_{22}a_{44} - a_{24}a_{42})\lambda^2 + (a_{21}a_{44} + a_{22}a_{43})\lambda + a_{21}a_{43} = 0$$

or

$$\lambda^4 + a_1\lambda^3 + a_2\lambda^2 + a_3\lambda + a_4 = 0. \tag{8}$$

The Hurwitz matrix for the above polynomial is

$$\begin{bmatrix} a_1 & 1 & 0 & 0 \\ a_3 & a_2 & a_1 & 1 \\ 0 & a_4 & a_3 & a_2 \\ 0 & 0 & 0 & a_4 \end{bmatrix}. \tag{9}$$

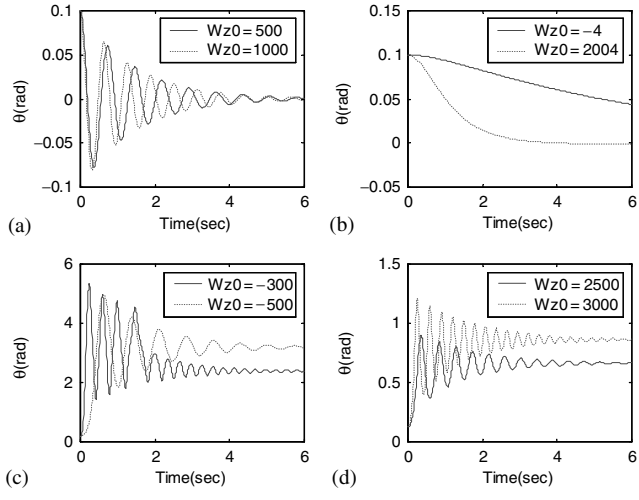

Figure 2. The numerical simulation of a two-axis gyro when ω_Z is constant.

The necessary and sufficient conditions for all the roots of characteristic equation to have negative real parts are provided by the Routh–Hurwitz criterion, i.e., the principle minors of the Hurwitz matrix must all be positive. So, the stability conditions are obtained as follows:

$$-a_{22} - a_{44} > 0, \quad \text{i.e., } d_1/(A + A_1) + d_2/(A + B_1 + A_2) > 0, \tag{10}$$

$$a_{22}a_{21} - a_{22}^2 a_{44} + a_{22}a_{24}a_{42} + a_{44}a_{43} - a_{22}a_{44}^2 + a_{44}a_{24}a_{42} > 0, \quad \text{i.e.,}$$

$$e_1\omega_{Z0}^2 + e_2\omega_{Z0} + e_3 > 0, \tag{11}$$

$$a_{22}a_{21}^2 a_{44} - a_{22}^2 a_{44}^2 a_{21} - a_{22}^3 a_{44}a_{43} + a_{22}a_{24}a_{42}a_{21}a_{44} + a_{24}a_{42}a_{22}^2 a_{43} + a_{44}a_{22}a_{43}^2$$

$$- a_{22}a_{44}^3 a_{21} - a_{22}^2 a_{44}^2 a_{43} + a_{24}a_{42}a_{21}a_{44}^2 + a_{44}a_{24}a_{42}a_{22}a_{43} - 2a_{21}a_{44}a_{22}a_{43} > 0, \text{ i.e.,}$$

$$e_4\omega_{Z0}^4 + e_5\omega_{Z0}^3 + e_6\omega_{Z0}^2 + e_7 w_{z0} + e_8 > 0, \tag{12}$$

$$a_{21}a_{43} > 0, \quad \text{i.e., } e_9\omega_{Z0}^4 + e_{10}\omega_{Z0}^3 + e_{11}\omega_{Z0}^2 + e_{12}\omega_{Z0}^4 + e_{13} > 0, \tag{13}$$

where e_i, $i = 1,2,\ldots,13$, are shown in Appendix C.

In the parameter values of gyro parameters [12, 13] are shown in Appendix A(II), from the above analysis, the motion is asymptotically stable when the following condition is held:

$$\omega_{Z01} = -4{\cdot}99 < \omega_{Z0} < \omega_{Z02} = 2004{\cdot}99, \tag{14}$$

i.e., inequalities (10)–(13) are satisfied.

From Figure 2(a), we see that the trajectory of the perturbed motion, which starts from the disturbances $\theta = 0{\cdot}1$ rad, asymptotically converges to the origin from the initial state when the condition $\omega_{Z01} < \omega_{Z0} < \omega_{Z02}$ is satisfied. From Figure 2(b), the trajectory of the perturbed motion converges to the origin but not oscillate when ω_{Z0} is near one of two limits (ω_{Z01} or ω_{Z02}). We can ensure that the system is local asymptotical stable when equation (14) is held. On the other hand, Figures 2(c) and 2(d) show that the trajectory moves far away from the origin. This means that the system is unstable. For the case in

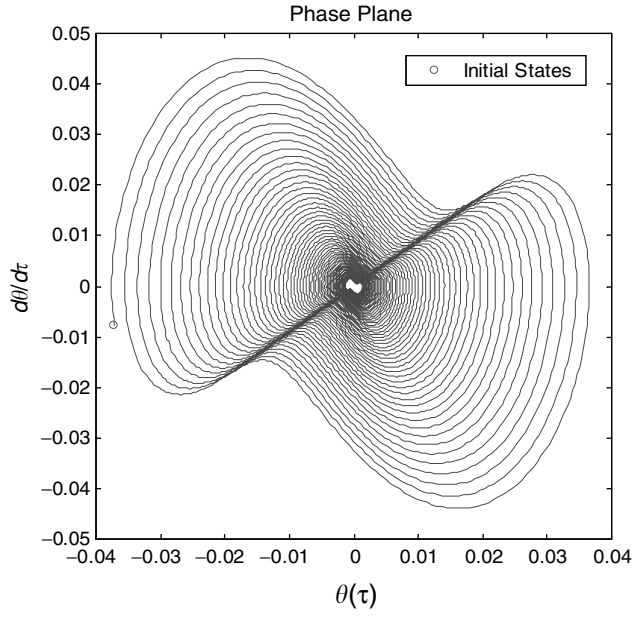

Figure 3. Stability analysis of a rate gyro at the origin for $f = 15$.

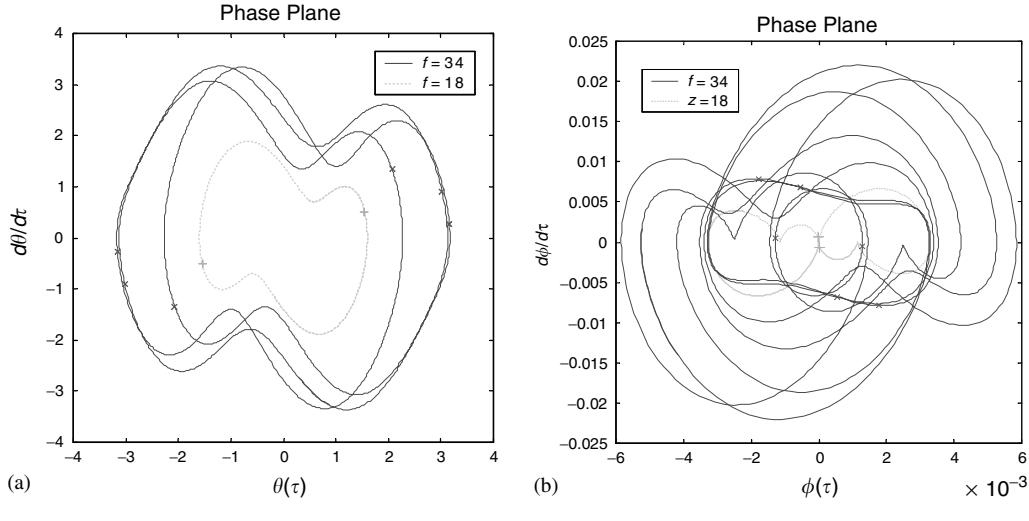

Figure 4. Two inversion-symmetric attractors of the system, (a) in the phase plane $\theta(\tau)$–$\dot{\theta}(\tau)$, (b) in the phase plane $\phi(\tau)$–$\dot{\phi}(\tau)$; a period-$2T$ attractor for $f = 18$, a period-$6T$ attractor for $f = 34$ where the symbols " + " and " × " indicate one period-T of $\omega_Z = f \sin \omega\tau$.

which ω_Z is time varying, the origin may be a stable equilibrium point in some conditions. In Figure 3, we obtain the trajectory corresponding to an asymptotical system in the phase plane by assuming that the amplitude of the sinusoidal angular velocity ω_Z below certain limits. When the amplitude of the sinusoidal angular velocityω_Z exceeds certain limits, the fixed point becomes limit cycle plotted in Figure 4 through Hopf bifurcation $f \approx 15{\cdot}4$.

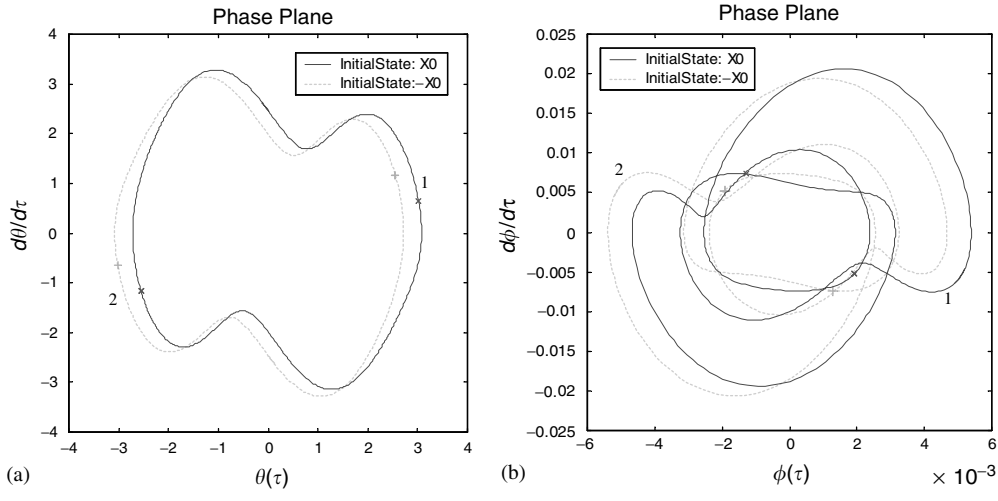

Figure 5. A dual period-2T attractor of the system, (a) in the phase plane $\theta(\tau)$–$\dot{\theta}(\tau)$, (b) in the phase plane $\phi(\tau)$–$\dot{\phi}(\tau)$ for $f = 31{\cdot}5$.

4. BIFURCATION ANALYSIS

For the case in which ω_Z is time varying, $\omega_Y = 0$ and $\omega_X = 0$, the origin is also an equilibrium point. However, as the following analysis, with the harmonic input with respect to the spin axis Z, i.e., $\omega_Z = f \sin \omega_f t$, the origin will become a hyperbolic closed orbit and the effects of parametric excitations gradually increase with the input amplitude increasing progressively. For convenience, the following parameters are used: the natural frequency of equation (1) $\omega_n = [k_1/(A + A_1)]^{1/2}$; frequency ratio $\omega = \omega_f/\omega_n$, where the exciting frequency is close to twice the natural frequency; time scale $\tau = \omega_n t$; damping ratio $\alpha_1 = d_1/[2(A + A_1)\omega_n]$, $\beta_1 = d_2/[2(A + B_1 + A_2)\omega_n]$; $\alpha_2 = H_c/[(A + A_1)\omega_n]$, $\beta_2 = k_2/[(A + B_1 + A_2)\omega_n^2]$, $\beta_3 = H_c/[(A + B_1 + A_2)\omega_n]$; equations (1)–(4) now can be simplified to

$$\ddot{\theta} + 2\alpha_1 \dot{\theta} + k\theta + \alpha_2 \dot{\phi} + NF_1(\theta, \phi, \tau) = 0, \tag{15}$$

$$\ddot{\phi} + 2\beta_1 \dot{\phi} + \beta_2 \phi - \beta_3 \dot{\theta} + NF_2(\theta, \phi, \tau) = 0, \tag{16}$$

where $k = 1$, $\dot{\theta} = \mathrm{d}\theta/\mathrm{d}\tau$, $\dot{\phi} = \mathrm{d}\phi/\mathrm{d}\tau$; $NF_1(\theta, \phi, \tau)$ and $NF_2(\theta, \phi, \tau)$, shown in Appendix D, represent the non-linear forcing function.

Räty [9] has shown that oscillators with external excitation and antisymmetric non-linear terms possess inversion-symmetric attractors with odd periods, i.e., non-linear terms $F(-x) = -F(x)$, the period of attractors: $T_j = (2j - 1)\, T_{sys} = (2j - 1)\, 2\pi/\omega_a$, where T_{sys} and ω_a are the period and the lowest angular frequency of attractors respectively. Similarly, the non-linear function $NF_1(\theta, \phi, \tau)$ and $NF_2(\theta, \phi, \tau)$ of the parametrically excited rate gyro suggest that these attractors are inversion-symmetric or inversions of each other corresponding to the varying parameter f. If the period of attractors of the system $T_j = (2j - 1)\, T_{sys}$ is of odd period, the non-linear forcing function of this system satisfies the relation:

$$NF_1(\theta(\tau), \phi(\tau), \tau) = -NF_1(-\theta(\tau), -\phi(\tau), \tau + T_j/2) = -NF_1(-\tilde{\theta}(\tau + T_j/2),$$
$$-\tilde{\phi}(\tau + T_j/2), \tau), \tag{17}$$

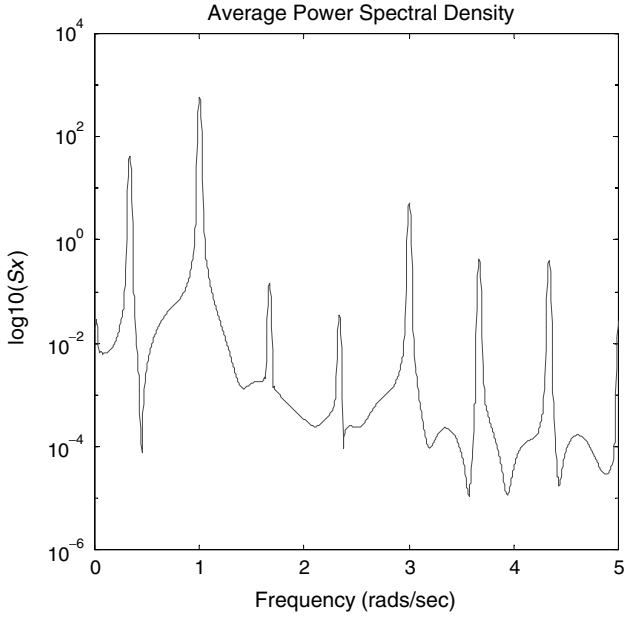

Figure 6. An average power spectrum of Figure 4 for $f = 34$.

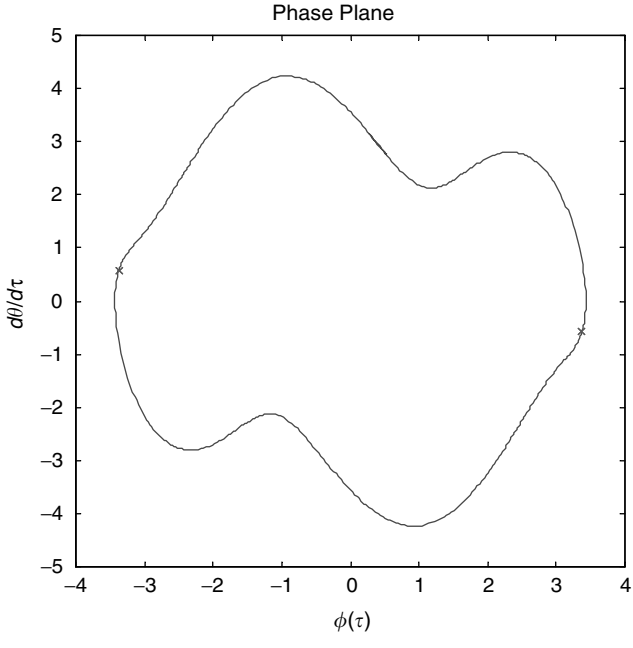

Figure 7. A symmetric period-$2T$ attractor of the system in the phase plane $\theta(\tau)$–$\dot{\theta}(\tau)$ for $f = 45$.

$$NF_2(\theta(\tau), \phi(\tau), \tau) = -NF_2(-\theta(\tau), -\phi(\tau), \tau + T_j/2) = -NF_2(-\tilde{\theta}(\tau + T_j/2), -\tilde{\phi}(\tau + T_j/2), \tau), \tag{18}$$

where $\theta(\tau)$, $\phi(\tau)$ and $\tilde{\theta}(\tau)$, $\tilde{\phi}(\tau)$ are the steady state solutions of equations (15) and (16) in the following relation: $\theta(\tau) = -\tilde{\theta}(\tau + T_j/2)$ and $\phi(\tau) = -\tilde{\phi}(\tau + T_j/2)$ implies the phase

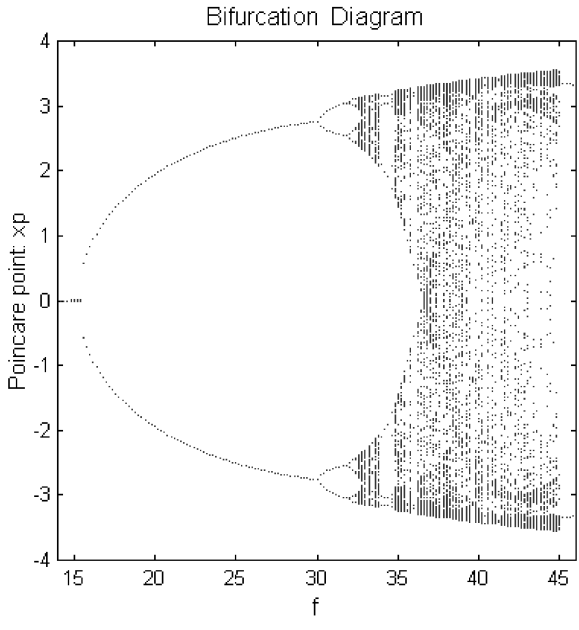

Figure 8. The bifurcation diagram.

portraits of attractors $\theta(\tau)$, $\phi(\tau)$ and $\tilde{\theta}(\tau)$, $\tilde{\phi}(\tau)$ with odd periods coincide together, i.e., $\theta(\tau) = \tilde{\theta}(\tau)$, $\phi(\tau) = \tilde{\phi}(\tau)$; the inversion-symmetric attractors are odd-period functions that coincide with the numerical simulation in period—$2T$ (period—T_1) and period—$6T$ (period—T_3) attractors as shown in Figure 4 where the symbols " + " and " × " indicate one period—T of function $\omega_Z(= f \sin \omega\tau)$. On the other hand, when the inversion symmetry is broken, it implies a pair of attractors $\theta(\tau)$, $\phi(\tau)$ and $\tilde{\theta}(\tau)$, $\tilde{\phi}(\tau)$ are inversions of each other, as illustrated in Figure 5.

5. NUMERICAL SIMULATIONS AND DISCUSSION

With the system parameter f varied, the system results obtained by numerical integration in the phase planes, Poincaré maps, average power spectra, bifurcations, and Lyapunov exponents diagrams. The trajectory of motion asymptotically converges to a hyperbolic fixed point at the origin, as shown in Figure 3 where $f = 15$, before the parameter $f \approx 15{\cdot}4$. After Hopf bifurcation, the original equilibrium point becomes unstable and a period—$2T$ stable symmetric limit cycle arises as shown in Figure 4, where $T = 2\pi/\omega$. A system with a symmetric non-linear function can undergo either a symmetry-breaking bifurcation for the symmetric solution of the system or a period-doubling bifurcation for the asymmetric solution of the system. When $f \approx 29{\cdot}5$, a symmetry-breaking bifurcation occurs. After this bifurcation, the original stable period—$2T$ attractor becomes unstable, a pair of stable period—$2T$ attractors arise and invert each other as shown in Figure 5 where $f = 31{\cdot}5$. As the parameter f increases further across $f \approx 32$, a stable periodic orbit appears with double the period of the original orbit, thereby indicating a period-doubling (flip) bifurcation. When the parameter is increased, a cascade of flip bifurcations occurs and leads to the onset of chaos. At $f \approx 34$, the chaotic attractor abruptly disappears and a period—$6T$ symmetric orbit appears, as shown in the phase plane and average power spectrum (see Figures 4 and 6).

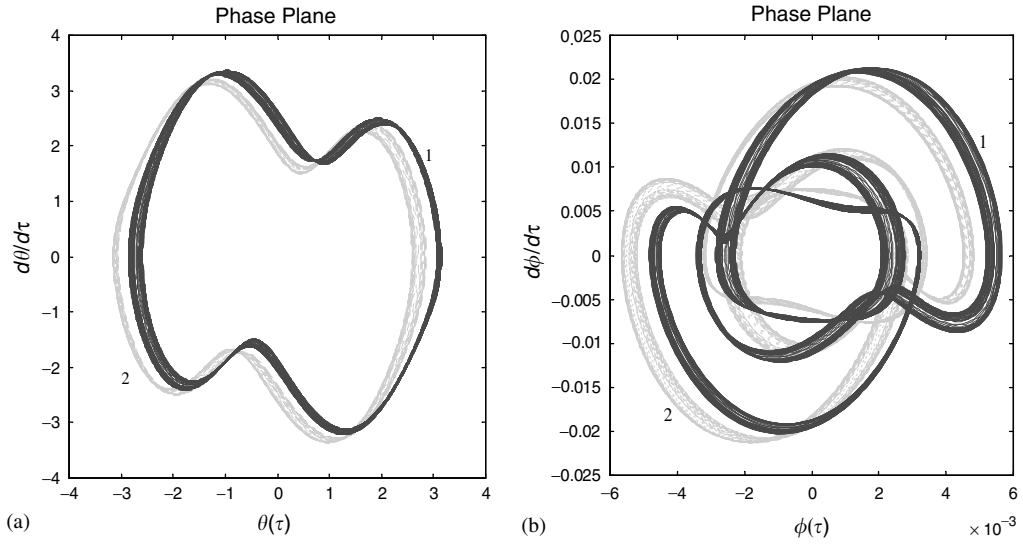

Figure 9. Two inverse chaotic attractors of the system, (a) in the phase plane $\theta(\tau)$–$\dot{\theta}(\tau)$, (b) in the phase plane $\phi(\tau)$–$\dot{\phi}(\tau)$ for $f = 32{\cdot}5$.

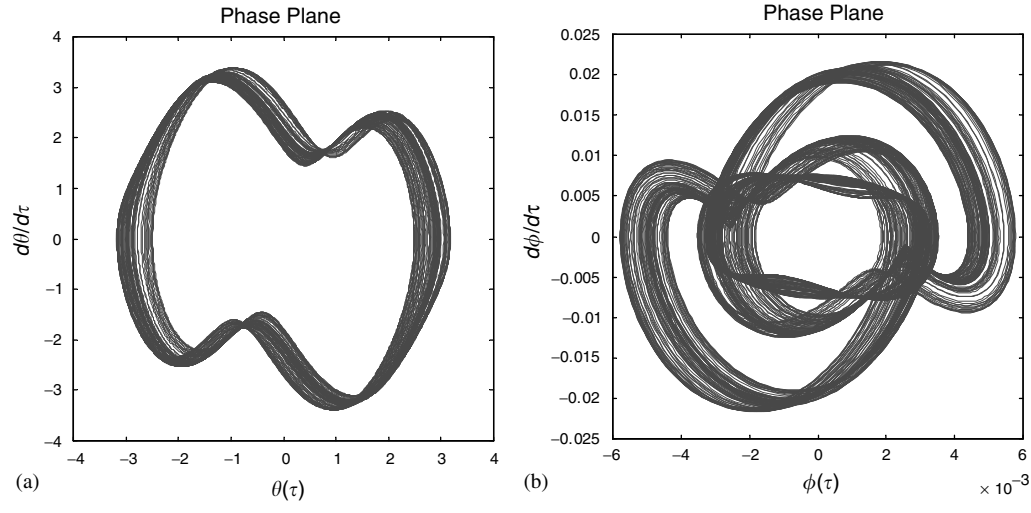

Figure 10. A chaotic attractor in conjunction with two chaotic attractors, (a) in the phase plane $\theta(\tau)$–$\dot{\theta}(\tau)$, (b) in the phase plane $\phi(\tau)$–$\dot{\phi}(\tau)$ for $f = 33$.

Indeed, for the large parameter $f = 45$, an inversion-symmetry period $-2T$ attractor is also obtained as shown in Figure 7.

To investigate bifurcation further, a Poincaré plane was used to display the bifurcation diagram, which shows Poincaré fixed points x_p plotted against the system parameter f. As the system parameter f is gradually increased through the parametric space, the bifurcation diagram obtained shows different types of bifurcations and chaos in Figure 8. The Hopf bifurcation at $f \approx 15{\cdot}4$, symmetry-breaking bifurcation at $f \approx 29{\cdot}5$, and period-doubling bifurcation at $f = 32$ are clearly shown. To investigate the periodic and chaotic motions in the bifurcation diagram further, the phase planes, Poincaré maps, and power spectra are

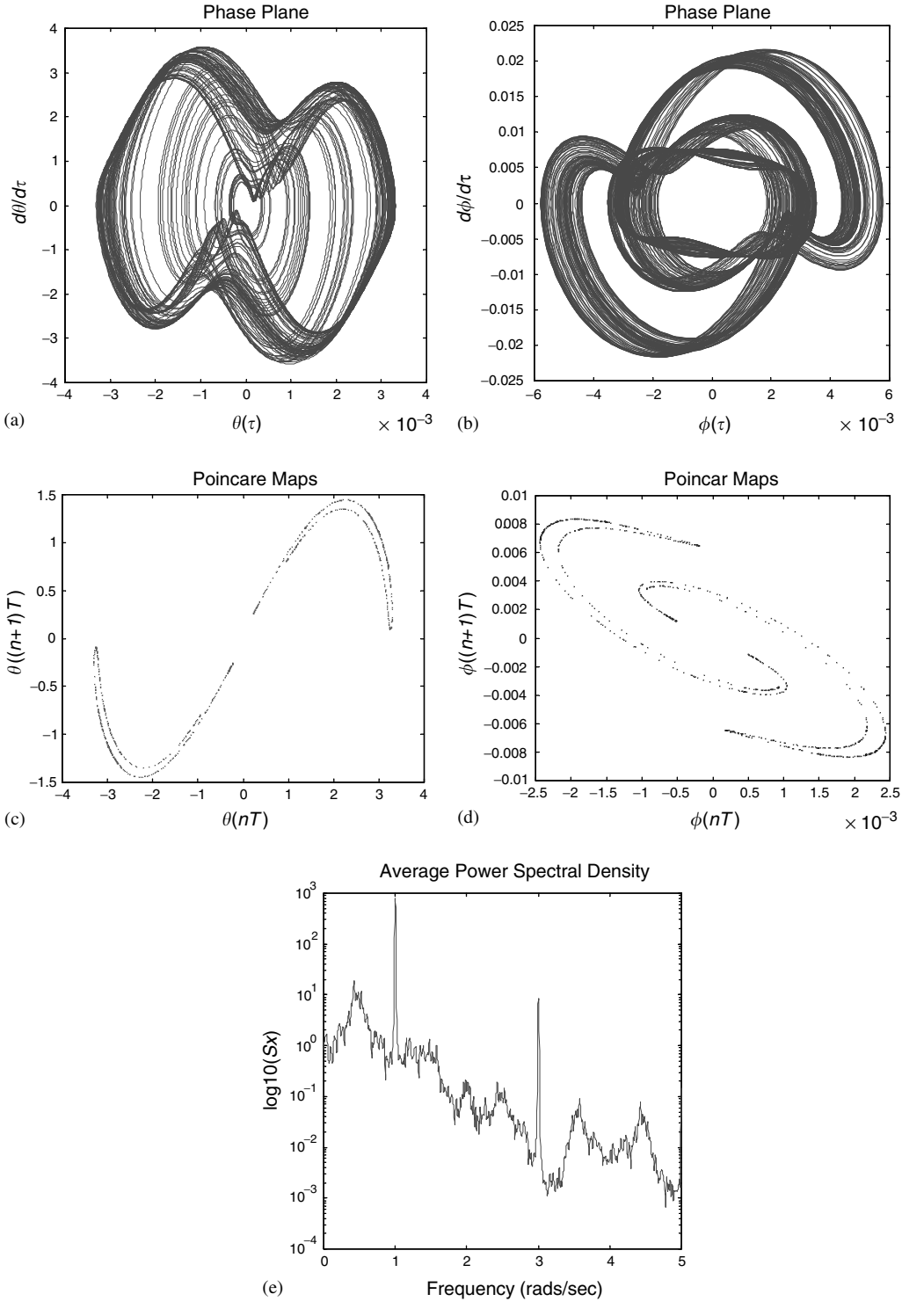

Figure 11. A symmetric chaotic attractor plotted in (a) the phase plane $\theta(\tau)$–$\dot{\theta}(\tau)$, (b) the phase plane $\phi(\tau)$–$\dot{\phi}(\tau)$, (c) the Poincaré maps $\theta(nT)$–$\theta((n+1)T)$, (d) the Poincaré maps $\phi(nT) - \phi((n+1)T)$, (e) the Average power spectrum for $f = 36{\cdot}3$.

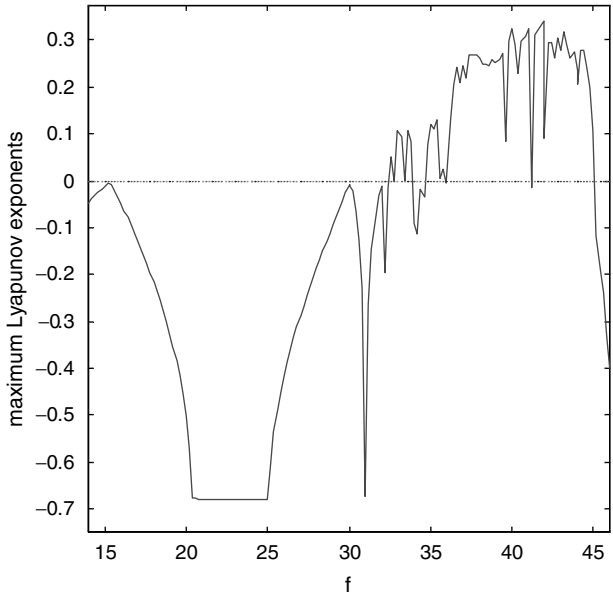

Figure 12. The largest Lyapunov exponents as a function of f.

used. After a cascade of period-doubling bifurcations, the dual response becomes chaotic rather than periodic for $f = 32{\cdot}5$, as shown in Figure 9. When $f = 33$, conjunction of the two inverse chaotic attractors creates a larger attractor, as shown in Figure 10. With the parameter increased, a large-amplitude chaotic motion appears in the phase plane, Poincaré map, and power spectrum as shown in Figure 11, where $f = 36{\cdot}3$. The power spectrum of a chaotic motion is a continuous board spectrum.

To confirm the chaotic dynamics, a qualitative and quantitative Lyapunov-exponent spectrum was performed. The algorithm for calculating the Lyapunov exponents was developed by Wolf *et al.* [16]. A spectrum of the largest Lyapunov exponent as a function of the parameter f is shown in Figure 12. As one of the Lyapunov exponents is positive, the motion is characterized as chaotic. When at least one Lyapunov exponent $\lambda_i = 0$ exists, motions are not stationary. For periodic motions, the Lyapunov exponents are non-positive and include only one zero Lyapunov exponent, while one negative exponent becomes zero when one type of periodic motion bifurcates to another.

For $f = 36{\cdot}3$, the Lyapunov exponents were found to be $\lambda_1 = 0{\cdot}171$, $\lambda_2 = 0$, $\lambda_3 = -0{\cdot}936$, $\lambda_4 = -0{\cdot}938$, $\lambda_5 = -1{\cdot}534$ and the Lyapunov dimension $d_L = 2{\cdot}183$ was also calculated using the relation proposed by Frederickson *et al.* [17]:

$$d_L = j + \sum_{i=1}^{j} \frac{\lambda_i}{|\lambda_{j+1}|},$$

where λ_1 is the largest Lyapunov exponent and j is the index of the smallest non-negative Lyapunov exponents. From the above discussion, it is evident that Lyapunov exponents are a measure of the fractal geometry of the attractor and the property of sensitivity dependence on initial conditions.

Physically, chaos may be desirable or undesirable, depending on the application. In mechanical systems, chaos may lead to irregular motions, so it has to be reduced or suppressed. In this case, we used a feedback constant control torque with the assistance of

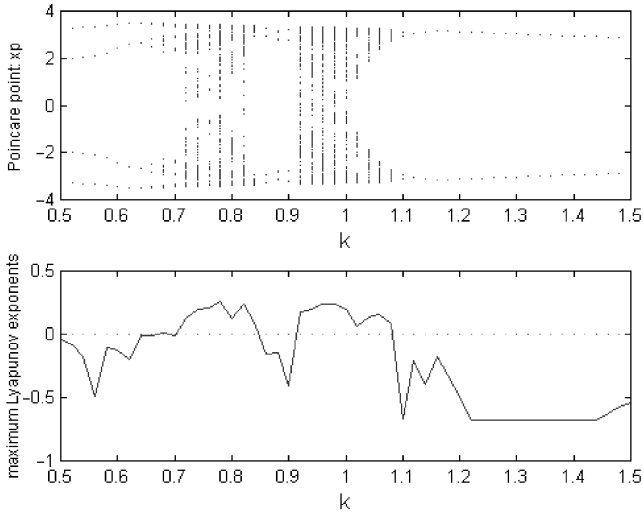

Figure 13. The bifurcation diagram and the largest Lyapunov exponent as a function of k.

the Lyapunov exponent calculations to bring the system from a chaotic regime to a regular. For changing the parameter k form 0·5 to 1·5, there are the bifurcation diagram and the spectrum of the largest Lyapunov exponents λ_{max} as the function of the stiffness coefficient k of equation (15) in Figure 13. As $\lambda_{max} < 0$ for the suitable k, the system is periodic.

6. CONCLUSIONS

In this paper, a two-axis rate gyro with sinusoidal velocity about its spin axis Z exhibits the non-linear characteristic of both sine, cos function and parametric excitation when the parameter is varied. For the autonomous case in which ω_Z is steady, the stability conditions were derived by the Routh–Hurwitz criterion. A variety of parametric studies were performed to analyze the behavior of periodic attractors route to chaos via distinct bifurcations by using the numerical simulations. The behaviors of a symmetry-breaking precursor to period-doubling bifurcations and a cascade of period-doubling route to chaos occurred in this system. The occurrence of the chaotic motion of the system is also detected by calculating bifurcation diagrams, power spectral diagrams and Lyapunov exponents. In addition, we consider a suitable feedback constant force torque to suppress chaos in the system by computing Lyapunov exponents.

ACKNOWLEDGMENTS

The authors to thank the referees for their valuable and helpful comments on this paper. The authors are grateful to the National Science Council, Republic of China, for supporting this research under Grant NSC 89-2218-E-164-001.

REFERENCES

1. A. H. NAYFEH and D. T. MOOK 1979 *Nonlinear Oscillations*. New York: John Wiley & Sons; Chapters 4 and 5.

2. J. GUCKENHEIMER and P. HOLMES 1986 *Nonlinear Oscillations, Dynamical Systems and Bifurcation of Vector Fields*. New York: Springer-Verlag; Chapters 4–7.
3. S. WIGGINS 1988 *Global Bifurcations and Chaos*. New York: Springer-Verlag; Chapter 4.
4. K. YAGASKI 1994 *Nonlinear Dynamics* **6**, 125–142. Chaos in a pendulum with feedback control.
5. N. E. SANCHEZ and A. H. NAYFEH 1990 *International Journal of Non-Linear Mechanics* **25**, 163–176. Prediction of bifurcations in a parametrically excited Duffing oscillator.
6. S. L. LAU, Y. K. CHEUNG and S. Y. WU 1982 *American Society of Mechanical Engineers Journal of Applied Mechanics* **49**, 849–853. A variable parameter incrementation method for dynamic instability of linear and nonlinear elastic systems.
7. S. L. LAU and S. W. YUEN 1991 *Computer Methods in Applied Mechanics and Engineering* **91**, 1109–1121.The Hopf bifurcation and limit cycle by the incremental harmonic balance method.
8. A. H. MACDONALD and M. PLISCHKE 1983 *Physical Review B* **27**, 201–211. Study of the driven damped pendulum: application to Josephson junctions and charge–density–wave systems.
9. J. V. B. RÄTY and H. M. ISOMÄKI 1984 *Physics Letters A* **103**, 289–292. Absence of inversion-symmetric limit cycles of even periods and the chaotic motion of duffing's oscillator.
10. S. N. SINGH 1984 *IEEE Transactions on Aerospace and Electronic Systems* **AES-20**, 119–127. Gyro motion boundedness under uncertain vehicle spin and acceleration.
11. Z. M. GE and C. J. CHEN 1992 *American Institute of Aeronautics and Astronautics Journal of Guidance, Control, and Dynamics* **15**, 1034-1036. Stability of a rate gyro.
12. Z. M. GE and H. H. CHEN 1996 *Journal of Sound and Vibration* **194**, 107–117. Bifurcations and chaos in a rate gyro with harmonic excitation. doi:10.1006/jsvi.1996.0384.
13. Z. M. GE and H. H. CHEN 1997 *Journal of Sound and Vibration* **200**, 121–137. Bifurcations and chaotic motions in a rate gyro with a sinusoidal velocity about the spin axis. doi:10.1006/jsvi.1996.0695.
14. Z. M. GE and H. H. CHEN 1998 *Journal of Sound and Vibration* **209**, 753–769. Double Degeneracy and chaos in a rate gyro with feedback control. doi:10.1006/jsvi.1997.1281.
15. L. MEIROVITCH 1970 *Methods of Analytical Dynamics*. New York: McGraw-Hill.
16. A. WOLF, J. B. SWIFT, H. L. SWINNEY and J. A. VASTANO 1985 *Physica D* **16**, 285–317. Determining Lyapunov Exponents From a Time Series.
17. FREDERICKSON, J. L. KAPLAN, E. D. YORKE and J. A. YORKE 1983 *Journal of Differential Equations* **49**, 185–207. The Lyapunov dimension of strange attractors.

APPENDIX A

(1) Let X, Y, Z be a set of axes attached to the platform, as depicted in Figure 1. We denote the column matrix corresponding to a system of co-ordinates X, Y, Z by using the gimbal axes ξ, η, ζ, so that the transformation from the X, Y, Z to the ξ, η, ζ system is written $\{\boldsymbol{\xi}\} = [\mathbf{R}]\{\mathbf{X}\}$, where $\{\boldsymbol{\xi}\} = [\xi, \eta, \zeta]^{\mathrm{T}}$, $\{\mathbf{X}\} = [X, Y, Z]^{\mathrm{T}}$, $[\mathbf{R}] = [\cos\phi, 0, \ -\sin\phi;\ \sin\theta \sin\phi, \cos\theta, \sin\theta\cos\phi;\ \cos\theta\sin\phi, \ -\sin\theta, \cos\theta\cos\phi]$.

If ω_X, ω_Y, ω_Z denote the angular velocity components of the platform the gimbal angular velocity become

$$\boldsymbol{\omega}_\xi = \dot{\theta} + \omega_X \cos\phi - \omega_Z \sin\phi,$$

$$\boldsymbol{\omega}_\eta = \dot{\phi}\cos\theta + \omega_X \sin\theta\sin\phi + \omega_Z \sin\theta\cos\phi + \omega_Y \cos\theta,$$

$$\boldsymbol{\omega}_\zeta = -\dot{\phi}\sin\theta + \omega_X \cos\theta\sin\phi + \omega_Z \cos\theta\cos\phi - \omega_Y \sin\theta.$$

The rotor has the angular velocity $\dot{\psi}$ relative to the gimbal, so that the angular velocity of the rotor in terms of components about the gimbal axes can be written as

$$\boldsymbol{\Omega}_\xi = \boldsymbol{\omega}_\xi, \qquad \boldsymbol{\Omega}_\eta = \boldsymbol{\omega}_\eta, \qquad \boldsymbol{\Omega}_\zeta = \boldsymbol{\omega}_\zeta + \dot{\psi}.$$

Denoting by A, A, C and A_1, B_1, C_1 the moments of inertia of the rotor and gimbal, respectively, about axes ξ, η, ζ and by A_2 the moments of outer gimbal about axis Y, we can

write the kinetic energy

$$T = 1/2\,[A(\boldsymbol{\Omega}_\xi^2 + \boldsymbol{\Omega}_\eta^2) + C\boldsymbol{\Omega}_\zeta^2 + A_1\boldsymbol{\omega}_\xi^2 + B_1\boldsymbol{\omega}_\eta^2 + C_1\boldsymbol{\omega}_\zeta^2 + A_2(\dot{\phi} + \omega_Y)^2].$$

The potential energy is simply

$$V = 1/2k_2\phi^2,$$

Whereas Rayleigh's dissipation function has the form

$$F = 1/2\,[d_1\dot{\theta}2 + d_2(\dot{\phi} + \omega_Y)^2].$$

Recalling that $L = T—V$, where L is the Lagrangian, and Lagrange's equations for a system with dissipative torques and motor torque T_c takes the form

$$(A + A_1)[\ddot{\theta} - (\omega_X \sin\phi + \omega_Z \cos\phi)\dot{\phi} + (\dot{\omega}_X \cos\phi - \dot{\omega}_Z \sin\phi)] - (A + B_1 - C_1)\boldsymbol{\omega}_\eta\boldsymbol{\omega}_\zeta$$

$$-(-\boldsymbol{\omega}_\eta)H_c + d_1\dot{\theta} = T_c,$$

$$\mathrm{d}/\mathrm{d}t\,[(A + B_1)\boldsymbol{\omega}_\eta \cos\theta - C_1\boldsymbol{\omega}_\zeta \sin\theta + A_2(\dot{\phi} + \omega_Y) - \sin\theta H_c] + d_2(\dot{\phi} + \omega_Y) + k_2\phi = 0,$$

$$\mathrm{d}/\mathrm{d}t\,[C(\boldsymbol{\omega}_\zeta + \dot{\psi})] = 0,$$

where $H_c = C(\boldsymbol{\omega}_\zeta + \dot{\psi}) = const.$

(II) *The values of gyro parameters*: $(A + A_1) = 54$ dyn cm s^2, $H_c = 10{\cdot}8 \times 10^4$ dyn cm s, $k_1 = 54 \times 10^4$ dyn cm/rad, $d_1 = 7560$ dyn cm/rad s, $(A + B_1) = 64$ dyn cm s^2, $C_1 = 10$ dyn cm s^2, $A_2 = 10$ dyn cm s^2, $k_2 = 54 \times 10^8$ dyn cm/rad, $d_2 = 7560$ dyn cm rad s.

APPENDIX B

$$F_1(x_1, x_2, x_3, x_4) = -(-(A + A_1)\cos(x_3)x_4\omega_{Z0} + (A + B_1 - C_1)x_4^2\cos(x_1)\sin(x_1)$$

$$-2(A + B_1 - C_1)x_4\cos^2(x_1)\cos(x_3)\omega_{Z0}$$

$$+(A + B_1 - C_1)\cos(x_3)\omega_{Z0}x_4 - (A + B_1 - C_1)\sin(x_1)\cos^2(x_3)\omega_{Z0}^2\cos(x_1)$$

$$+k_1x_1 + \cos(x_1)H_cx_4$$

$$+H_c\sin(x_1)\cos(x_3)\omega_{Z0} + d_1x_2)/(A + A_1),$$

$$F_2(x_1, x_2, x_3, x_4) = -(d_2x_4 + k_2x_3 - \cos(x_1)x_2H_c + \cos(x_1)\sin(x_3)\omega_{Z0}H_c$$

$$+(A + B_1)\sin(x_3)\omega_{Z0}^2\cos(x_3) - (A + B_1 - C_1)\sin(x_3)\omega_{Z0}^2\cos(x_3)\cos^2(x_1)$$

$$-(A + A_1)\cos(x_3)\omega_{Z0}^2\sin(x_3) + (A + A_1)\cos(x_3)\omega_{Z0}x_2$$

$$-2(A + B_1 - C_1)\cos(x_1)x_4\sin(x_1)x_2 + 2(A + B_1 - C_1)\cos^2(x_1)x_2\cos(x_3)\omega_{Z0}$$

$$-(A + B_1 - C_1)x_2\cos(x_3)\omega_{Z0})/((A + B_1)\cos^2(x_1) + C_1\sin^2(x_1) + A_2).$$

APPENDIX C

$$e_1 = (- d_1/D_1^2D_2 - d_2/D_3^2D_4 + d_1/D_1^2D_5^2/D_3 + d_2/D_3^2D_5^2/D_1),$$

$$e_2 = (d_1/D_1^2H_c - 2d_1/D_1^2H_cD_5/D_3 + d_2/D_3^2H_c - 2d_2/D_3^2H_c/D_1D_5),$$

$$e_3 = d_1/D_1^2k_1 + d_1/D_1d_2^2/D_3^2 + d_1^2/D_1^2d_2/D_3 + d_1/D_1^2H_c^2/D_3 + d_2/D_3^2k_2 + d_2/D_3^2H_c^2/D_1,$$

$$\begin{aligned} e_4 = {} & (- d_1/D_1^3D_5^2/D_3^2D_2d_2 - D_5^2/D_1^2/D_3^3D_2d_2^2 - D_5^2/D_1^3/D_3^2d_1^2D_4 + d_2/D_3^3d_1/D_1D_4^2 \\ & + d_1/D_1^3D_2^2d_2/D_3 - d_2/D_3^3D_5^2/D_1^2d_1D_4 - 2D_2/D_1^2d_2/D_3^2d_1D_4), \end{aligned}$$

$$\begin{aligned} e_5 = {} & (2H_c/D_1^3D_5/D_3^2d_1^2D_4 + D_5^2/D_1^3/D_3^2d_1^2H_c + 2d_2/D_3^3H_c/D_1^2D_5d_1D_4 + d_2/D_3^3D_5^2/D_1^2d_1H_c \\ & - 2d_2/D_3^3d_1/D_1H_cD_4 \\ & + (2d_1/D_1^3H_cD_5/D_3^2D_2 + d_1/D_1^3D_5^2/D_3^2H_c)d_2 + 2H_c/D_1^2d_2/D_3^2d_1D_4 \\ & + 2D_2/D_1^2d_2/D_3^2d_1H_c \\ & + (2H_c/D_1^2D_5/D_3^3D_2 + D_5^2/D_1^2/D_3^3H_c)d_2^2 - 2d_1/D_1^3H_cD_2d_2/D_3), \end{aligned}$$

$$\begin{aligned} e_6 = {} & (- d_1^3/D_1^3d_2/D_3^2D_4 - d_1/D_1^2d_2^2/D_3^3D_2 - H_c^2/D_1^3/D_3^2d_1^2D_4 - 2H_c^2/D_1^3D_5/D_3^2d_1^2 \\ & + D_5^2/D_1^3/D_3^2d_1^2k_2 + d_2/D_3^3d_1/D_1(- 2k_2D_4 + H_c^2) - d_1^2/D_1^3d_2^2/D_3^2D_2 \\ & + (- d_1/D_1^3H_c^2/D_3^2D_2 - 2d_1/D_1^3H_c^2D_5/D_3^2 + d_1/D_1^3D_5^2/D_3^2k_1)d_2 \\ & - d_1^2/D_1^2d_2^2/D_3^3D_4 + 2k_1/D_1^2d_2/D_3^2d_1D_4 - 2H_c^2/D_1^2d_2/D_3^2d_1 \\ & + 2D_2/D_1^2d_2/D_3^2d_1k_2 - d_2/D_3^3H_c^2/D_1^2d_1D_4 - 2d_2/D_3^3H_c^2/D_1^2D_5d_1 + d_2/D_3^3D_5^2/D_1^2d_1k_2 \\ & + (- H_c^2/D_1^2/D_3^3D_2 - 2H_c^2/D_1^2/D_3^3D_5 \\ & + D_5^2/D_1^2/D_3^3k_1)d_2^2 + d_1/D_1^3(- 2k_1D_2 + H_c^2)d_2/D_3), \end{aligned}$$

$$\begin{aligned} e_7 = {} & (d_1/D_1^2d_2^3/D_3^3H_c + (H_c^3/D_1^2/D_3^3 - 2H_c/D_1^2D_5/D_3^3k_1)d_2^2 + 2d_1/D_1^3k_1H_cd_2/D_3 \\ & + 2d_2/D_3^3d_1/D_1k2H_c + d_1^2/D_1^3d_2^2/D_3^2H_c + H_c^3/D_1^3/D_3^2d_1^2 - 2H_c/D_1^3D_5/D_3^2d_1^2k_2 \\ & + d_1^3/D_1^3d_2/D_3^2H_c + (d_1/D_1^3H_c^3/D_3^2 - 2d_1/D_1^3H_cD_5/D_3^2k_1)d_2 \\ & + d_1^2/D_1^2d_2^2/D_3^3H_c + d_2/D_3^3H_c^3/D_1^2d_1 - 2d_2/D_3^3H_c/D_1^2D_5d_1k_2 \\ & - 2k_1/D_1^2d_2/D_3^2d_1H_c - 2H_c/D_1^2d_2/D_3^2d_1k_2), \end{aligned}$$

$$\begin{aligned} e_8 = {} & d_1/D_1^3k_1^2d_2/D_3 + d_1^2/D_1^3d_2^2/D_3^2k_1 - 2k_1/D_1^2d_2/D_3^2d_1k_2 + H_c^2/D_1^3/D_3^2d_1^2k_2 + d_1^3/D_1^3d_2/D_3^2k_2 \\ & + d_1/D_1^2d_2^3/D_3^3k_1 + H_c^2/D_1^2/D_3^3k_1d_2^2 + d_1/D_1^3H_c^2/D_3^2k_1d_2 + d_1^2/D_1^2d_2^2/D_3^3k_2 \\ & + d_2/D_3^3d_1/D_1k_2^2 + d_2H_c^2/D_3^3/D_1^2d_1k_2, \end{aligned}$$

$$e_9 = D_2/D_1D_4/D_3,$$

$$e_{10} = (-H_c/D_1D_4 - D_2/D_1H_c)/D_3,$$

$$e_{11} = (-k_1/D_1D_4 + H_c^2/D_1 - D_2/D_1k_2)/D_3,$$

$$e_{12} = (k_1/D_1H_c + H_c/D_1k_2)/D_3,$$

$$e_{13} = k_1/D_1k_2/D_3,$$

where $D_1 = (A + A_1)$, $D_2 = (A + B_1 - C_1)$, $D_3 = (A + B_1 + A_2)$, $D_4 = (A + A_1 - C_1)$, $D_5 = (2A + A_1 + B_1 - C_1)$.

APPENDIX D

$$\begin{aligned}
NF_1(\theta,\phi,\tau) = & -(A + B_1 - C_1)(-\dot{\phi}c_2\omega_{Zt}\omega_n + (-\omega_n^2\dot{\phi}^2 s_1 + s_1c_2^2\omega_{Zt}^2 \\
& + 2\dot{\phi}c_2\omega_{Zt}\omega_n c_1)c_1)/[(A + A_1)\omega_n^2] \\
& - H_c(-\omega_n\dot{\phi}c_1 - s_1c_2\omega_{Zt} + \dot{\phi}\omega_n)/[(A + A_1)\omega_n^2] - (\dot{\phi}c_2\omega_{Zt}\omega_n + s_2\omega_n\dot{\omega}_{Zt})/\omega_n^2, \\
NF_2(\theta,\phi,\tau) = & ((s_1^2\dot{\theta}c_2\omega_{Zt}\omega_n A_2 - k_2\phi s_1^2 - \dot{\phi}d_2\omega_n s_1^2)C_1 + (-\omega_{Zt}^2 s_2 A_2 + \omega_{Zt}\dot{\theta}\omega_n A_2)c_2(A + A_1) \\
& + (2C_1s_1\dot{\phi} \times \dot{\theta}\omega_n^2 A_2 - C_1s_1c_2\dot{\omega}_{Zt}\omega_n A_2 + (-\omega_{Zt}\dot{\theta}\omega_n A_2 + \omega_{Zt}^2 s_2 A_2)c_2C_1c_1)c_1 \\
& + (\dot{\theta}\omega_n C_1 s_1^2 + \dot{\theta}\omega_n A_2 \\
& + (s_2\omega_{Zt}A_2 - \dot{\theta}\omega_n A_2)c_1)H_c + (k_2\phi + (-s_1^2\dot{\theta}\omega_{Zt}\omega_n A_2 + s_1^2 s_2\omega_{Zt}^2 A_2)c_2 \\
& + \dot{\phi}d_2\omega_n + C_1s_1^2\dot{\theta}c_2\omega_{Zt}\omega_n \\
& + (-\omega_{Zt}^2 s_2 + \omega_{Zt}\dot{\theta}\omega_n)c_2(A + A_1) + (-2s_1\dot{\phi}\dot{\theta}\omega_n^2 A_2 + 2C_1s_1\dot{\phi}\dot{\theta}\omega_n^2 \\
& + (s_1c_2\omega_n A_2 - C_1s_1c_2\omega_n)\dot{\omega}_{Zt} \\
& + (-k_2\phi + c_2\omega_{Zt}\dot{\theta}\omega_n A_2 - \dot{\phi}d_2\omega_n \\
& + (\omega_{Zt}^2 s_2 - \omega_{Zt}\dot{\theta}\omega_n)c_2C_1)c_1)c_1 + (s_2\omega_{Zt} - \dot{\theta}\omega_n \\
& + c_1\dot{\theta}\omega_n)c_1H_c + ((s_1^2 s_2\omega_{Zt}^2 - s_1^2\dot{\theta}\omega_{Zt}\omega_n)c_2 + (-2s_1\dot{\phi}\dot{\theta}\omega_n^2 + s_1c_2\dot{\omega}_z\omega_n \\
& + c_2\omega_{Zt}\dot{\theta}\omega_n c_1)c_1)(A + B_1))(A + B_1))/[((A + B_1)c_1^2 \\
& + C_1s_1^2 + A_2)(A + B_1 + A_2)\omega_n^2],
\end{aligned}$$

where $s_1 = \sin\theta$, $s_2 = \sin\phi$, $c_1 = \cos\theta$, $c_2 = \cos\phi$, etc. $\omega_{Zt} = f\sin\omega\tau$, $\omega = \omega_f/\omega_n$, $\dot{\omega}_{Zt} = \mathrm{d}\omega_{Zt}/\mathrm{d}\tau$.